Classical interatomic potentials for Si-O-F and Si-O-Cl systems

AUTHOR(S):

Ohta, H; Hamaguchi, S

CITATION:

Ohta, H ...[et al]. Classical interatomic potentials for Si-O-F and Si-O-Cl systems. JOURNAL OF CHEMICAL PHYSICS 2001, 115(14): 6679-6690

ISSUE DATE:

2001-10-08

URL:

http://hdl.handle.net/2433/50272

Classical interatomic potentials for Si–O–F and Si–O–Cl systems

H. Ohta[a] and S. Hamaguchi[b]
Department of Fundamental Energy Science, Kyoto University, Gokasho, Uji, Kyoto 611-0011, Japan

(Received 7 May 2001; accepted 16 July 2001)

Stillinger–Weber (SW)-type potential sets have been developed for Si–O–F and Si–O–Cl systems based on interatomic potential energy data obtained from *ab initio* quantum-mechanical calculations. We have constructed the new potential sets in such a way that the obtained potentials are supersets of existing well-known SW-type potentials for Si, SiO_2, and Si-halogen systems. Our aim of the potential development is to perform molecular dynamics (MD) simulations for both silicon and silicon dioxide etching by F or Cl on the same footing. Presented in this article are details of the potential derivation and some sample MD simulation results. © *2001 American Institute of Physics.* [DOI: 10.1063/1.1400789]

I. INTRODUCTION

Plasma processing such as reactive ion etching (RIE) and plasma-enhanced chemical vapor deposition (PECVD) are widely used in the semiconductor industry. As the dimensions of microelectronic devices diminish, atomic-scale control of semiconductor manufacturing processes has become increasingly important. Better understanding of surface reaction dynamics can facilitate the development of such atomic-scale process control techniques.

Molecular-dynamics (MD) simulation may be used to study surface reaction dynamics for various processes. For plasma processing, where relatively high-energy ionic and/or atomic species are involved, the number of simulation particles required for realistic simulations can be very large. Therefore, for MD simulations of plasma–surface interactions, it is not practical to resolve electron dynamics of each atom using quantum mechanical calculations at every time step of atomic motion. So we employ classical MD simulation in this work, where interatomic potential functions are specified in advance.

One of the most important issues regarding classical MD simulation is how to determine the interatomic potentials. As to materials used for plasma etching processes, several potential functions have been proposed by various investigators. Classical multibody potentials for Si and F systems in the form of a cluster expansion were first developed by Stillinger and Weber.[1,2] Feil *et al.* extended the same functional form [i.e., Stillinger–Weber (SW) potential] to Si and Cl systems.[3] These potential functions are designed to reproduce some structural and thermodynamical characteristics of the materials (such as stress and melting temperatures) and relevant structural chemistry for some selected molecules composed of these elements. To date many researchers have performed classical MD simulations using these potentials to study plasma–surface interactions for Si etching by halogens.[4–11] The obtained simulation results have been in reasonable agreement with experimental observations. These simulations have demonstrated their usefulness in a relatively high-energy range (e.g., from a few dozen to a few hundred eV) appropriate for plasma or beam etching.

To represent lower energy phenomena such as adsorption and surface diffusion with high accuracy, more precise potentials may be required. Weakliem *et al.* and Carter *et al.*[12–14] have modified the original SW potentials for Si–F systems using interatomic potential data obtained from *ab initio* quantum-mechanical calculations to perform MD simulations of fluorine adsorption on silicon. Their simulation results have indicated that the original SW potentials do not necessarily describe the reaction paths correctly and demonstrated the effectiveness of using *ab initio* data to construct and/or modify interatomic potentials.

Empirically obtained potential functions such as the original SW potentials are designed to reproduce only relatively stable atomic configurations and, in general, there is no guarantee that the functions give accurate interatomic potential energy values for all possible atomic configurations. Such inaccuracy may lead to unrealistic results in MD simulations especially in a low kinetic-energy regime, where chemical effects dominate atomic interactions. Recently Hanson *et al.* have modified the SW potentials for Si–Cl systems by adding new terms, i.e., an embedding term and a four-body term based on *ab initio* data[15] in order to represent realistic surface reactions during plasma etching.

The classical potentials described above (including the original SW potentials) have been used to simulate Si etching by halogens. For simulation of interactions between silicon dioxide and halogens, however, no classical interatomic potential was previously available. To the best of the authors' knowledge, prior to our simulations presented in Ref. 11 and this article, oxide etching simulations were performed only for pure physical sputtering by Ar atoms.[16,17]

The interatomic potentials for SiO_2 systems have been proposed by several investigators.[18–20] Interaction with an Ar atom may be treated as two-body interaction using, e.g., Moliére repulsive pair potential.[21] It is relatively easy to incorporate a two-body potential with other multibody interatomic potentials. Although classical interatomic potentials for Si–F, Si–Cl, and Si–O systems were separately devel-

[a]Electronic mail: ohta@center.iae.kyoto-u.ac.jp
[b]Electronic mail: hamaguch@energy.kyoto-u.ac.jp

oped before, development of interatomic potentials for the combined system requires construction of additional interatomic potential functions. The goal of this work is to present the derivation of new classical potential sets that can be used to simulate SiO_2 etching by halogen beams or plasmas.

In order to simplify the potential development process, we make use of existing classical potentials for Si–F[1,2] and Si–Cl[3] systems. For Si–O systems, we use a SW-type potential set developed by Watanabe *et al.*[20] Assuming the SW-type functional forms can be extended to Si–O–F or Si–O–Cl systems, we have developed potential functions that are reducible to the previously obtained potentials in the corresponding cases. In other words, we employ SW-type potential functions that include the previously obtained SW-type potentials for Si–F or Si–Cl and Si–O systems as subsets and determine the remaining unknown parameters by nonlinearly fitting the functions to interatomic potential energy data obtained from *ab initio* quantum-mechanical calculations.

II. DERIVATION OF CLASSICAL POTENTIALS

A. Stillinger–Weber-type potential functions

In this section, we derive SW-type potential functions for Si–O–Cl and Si–O–F systems. Here we consider atomic interactions only among charge neutral species. Suppose that the total energy of atomic systems is expressed by the summation of two- and three-body potentials as

$$\Phi=\sum_{i<j} v_2(i,j)+\sum_{i<j<k} v_3(i,j,k). \tag{1}$$

Following Stillinger and Weber,[1] we assume that the pairlike interaction $v_2(i,j)$ between the ith and jth atoms has the form

$$v_2(i,j)\equiv v_{ij}(r_{ij})=g(i,j)A_{ij}\left(\frac{B_{ij}}{r_{ij}^{p_{ij}}}-\frac{1}{r_{ij}^{q_{ij}}}\right)\exp\left(\frac{C_{ij}}{r_{ij}-a_{ij}}\right) \quad \text{if} \quad r_{ij}<a_{ij}, \tag{2}$$

and $v_2(i,j)=0$ otherwise. Here $r_{ij}=|\mathbf{r}_j-\mathbf{r}_i|$ denotes the distance between the ith and jth atoms located at $\mathbf{r}_i$ and $\mathbf{r}_j$. The parameters A_{ij}, B_{ij}, C_{ij}, p_{ij}, q_{ij}, and a_{ij} depend only on the species (i.e., element types) of ith and jth atoms. (In this paper, indices i, j,..., etc., appearing as subscripts or superscripts of a quantity indicate that the quantity depends only on the species of corresponding atoms unless otherwise specified.) The cut-off distance is denoted by a_{ij}. Function $g(i,j)$ is designed to reproduce the appropriate valence of oxygen, which will be discussed in the following subsection. The system symmetry requires the invariance of parameters under the exchange of indices i and j, i.e., $g(i,j)=g(j,i)$ $A_{ij}=A_{ji}$,..., etc.

To assure the symmetry of the potential function, it may be more convenient to decompose the three-body term $v_3(i,j,k)$ in Eq. (1) into three parts[1] as

$$\begin{aligned} v_3(i,j,k)&\equiv v_{ijk}(\mathbf{r}_i,\mathbf{r}_j,\mathbf{r}_k)\\ &=h_{jik}(r_{ij},r_{ik},\theta_{jik})+h_{ijk}(r_{ji},r_{jk},\theta_{ijk})\\ &\quad+h_{ikj}(r_{ki},r_{kj},\theta_{ikj}), \end{aligned}$$

with θ_{jik} being the angle spanned by vectors $\mathbf{r}_{ij}\equiv\mathbf{r}_j-\mathbf{r}_i$ and $\mathbf{r}_{ik}\equiv\mathbf{r}_k-\mathbf{r}_i$ at vertex $\mathbf{r}_i$.

To construct interatomic potentials for Si–O–F (or Si–O–Cl) systems, we employ the functional form[1] for h_{jik} given by either

$$h_{jik}(r,s,\theta)=\lambda_{jik}\exp\left[\frac{\gamma_{jik}^{j}}{r-a_{jik}^{j}}+\frac{\gamma_{jik}^{k}}{s-a_{jik}^{k}}\right], \tag{3}$$

or

$$h_{jik}(r,s,\theta)=\lambda_{jik}\exp\left[\frac{\gamma_{jik}^{j}}{r-a_{jik}^{j}}+\frac{\gamma_{jik}^{k}}{s-a_{jik}^{k}}\right]\times|\cos\theta-\cos\theta_{jik}^{0}|^{2\alpha_{jik}}, \tag{4}$$

depending on the species of ith atom if $r<a_{jik}^{j}$ and $s<a_{jik}^{k}$. Otherwise $h_{jik}=0$. Here λ_{jik}, γ_{jik}^{j}, γ_{jik}^{k}, a_{jik}^{j}, a_{jik}^{k}, θ_{jik}^{0}, and α_{jik} are parameters that depends on the species of (i,j,k) triplet. The cut-off distances are denoted by a_{jik}^{j} and a_{jik}^{k}. The system symmetry requires these parameters to be invariant under the exchange of the first and third indices of the subscripts, e.g., $\lambda_{jik}=\lambda_{kij}$, $\gamma_{jik}^{j}=\gamma_{kij}^{j}$,..., *et al.* We have modified the original SW function by introducing a new parameter α_{jik} in order to improve parameter fitting. Equation (3) is employed if the atom denoted by the second index of subscripts (i.e., the ith atom) is either Cl or F. This function effectively introduces the single valence of a halogen atom by shielding attractive forces arising from the two-body potentials. Equation (4) is employed if the ith atom is either Si or O. This potential is designed to restrict configuration numbers around the ith atom and to reproduce appropriate bond angles for the covalent binding. Following Ref. 1, we also use other potential functions for some special cases, as given in Appendix A.

The potential set for Si–O-halogen systems may be divided into four subsets, i.e., potentials for (a) Si–halogen systems, (b) Si–O systems, (c) O–halogen systems, and (d) systems containing Si, O, and halogen atoms. For Si–

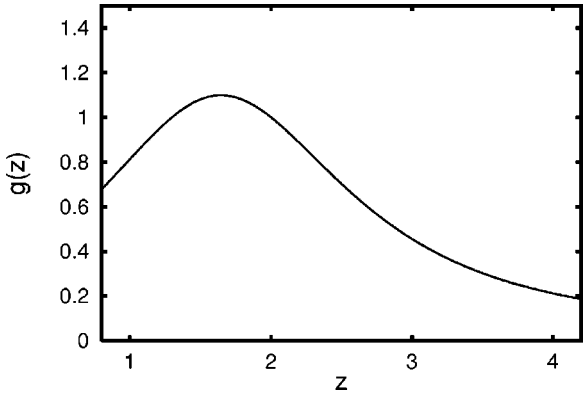

FIG. 1. Bond softening function $g(z)$ given in Eq. (7).

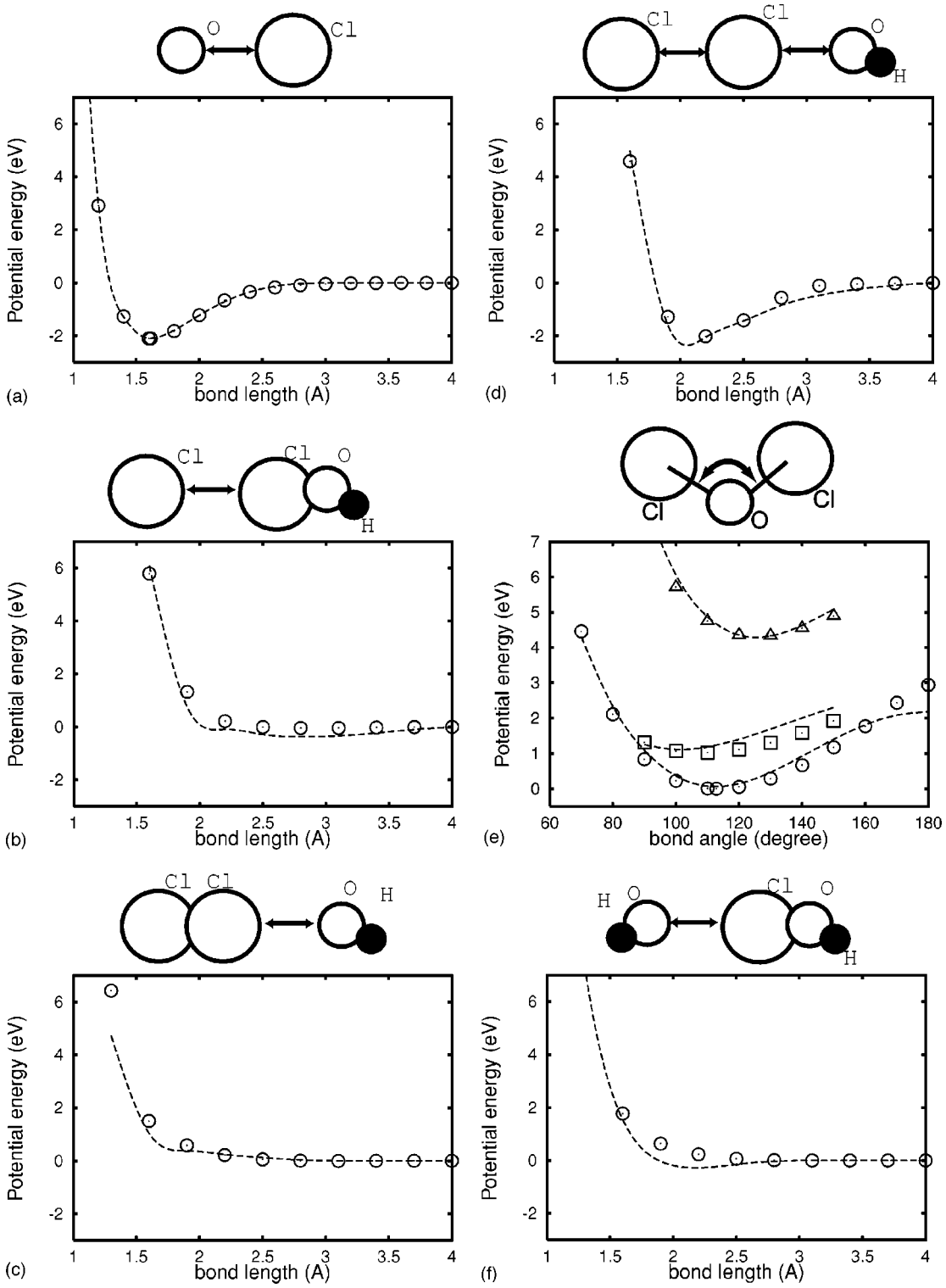

FIG. 2. Potential energy data for Cl–O systems obtained from *ab initio* calculations (○, □, and △) and our potential functions (dotted lines). The atomic configuration used for the energy calculations is shown above each figure. The arrows (↔) indicate variable parameters (i.e., bond lengths or angles). In (d) both Cl–Cl and Cl–O bond lengths are varied simultaneously. In (e) the selected bond lengths of O–Cl are 1.40 Å (△), 1.7343 Å (○), and 2.00 Å (□).

halogen systems, we use the original SW potentials developed by Stillinger and Weber for Si–F systems[1,2] and also the SW potentials by Feil for Si–Cl systems.[3] As to the potentials for Si–O systems, we use the SW-type potentials developed by Watanabe *et al.*[20] For the remaining (c) and (d) above, we determine the potential set using potential data obtained from *ab initio* calculations.

Note that Watanabe *et al.* did not consider O–O bond and modeled the O–O interaction only by a repulsive pair force. Accordingly three-body functions h_{jik} that directly account for the O–O interaction are also set to be 0, i.e., $h_{\mathrm{SiOO}}=h_{\mathrm{OOO}}=0$. Following Watanabe *et al.*, we also employ the same potential for the O–O interaction and extended it to Si–O–Cl or Si–O–F systems, assuming $h_{\mathrm{ClOO}}=h_{\mathrm{FOO}}=0$,

TABLE I. Parameters of the interatomic potential functions for Cl–O and F–O systems.

Si–O–Cl			Si–O–F		
v_{ClO}	A_{ClO}	71.0	v_{FO}	A_{FO}	142.5
[Eq. (2)]	B_{ClO}	0.471	(Eq. 2)	B_{FO}	0.2772
	C_{ClO}	3.55		C_{FO}	4.111
	p_{ClO}	3.13		p_{FO}	3.0
	q_{ClO}	1.53		q_{FO}	1.0
	a_{ClO}	1.8		a_{FO}	1.6
	R_{ClO}	1.0		R_{FO}	0.9
	D_{ClO}	0.1		D_{FO}	0.1
h_{ClClO}	λ_{ClClO}	1170	h_{FFO}	λ_{FFO}	1.135×10^6
[Eq. (3)]	γ^{Cl}_{ClClO}	3.97	[Eq. (3)]	γ^{F}_{FFO}	13.44
	γ^{O}_{ClClO}	3.24		γ^{O}_{FFO}	3.441
	a^{Cl}_{ClClO}	2.0862		a^{F}_{FFO}	2.0862
	a^{O}_{ClClO}	1.8		a^{O}_{FFO}	1.6
h_{ClOCl}	λ_{ClOCl}	78.3	h_{FOF}	λ_{FOF}	4720
[Eq. (4)]	γ^{Cl}_{ClOCl}	1.83	[Eq. (4)]	γ^{F}_{FOF}	3.608
	a^{Cl}_{ClOCl}	1.8		a^{F}_{FOF}	1.6
	$\cos\theta^0_{ClOCl}$	−0.221		$\cos\theta^0_{FOF}$	−0.048 24
	α_{ClOCl}	1.0		α_{FOF}	1.285
h_{OClO}	λ_{OClO}	1.66×10^5	h_{OFO}	λ_{OFO}	3.092×10^4
[Eq. (3)]	γ^{O}_{OClO}	5.78	[Eq. (3)]	γ^{O}_{OFO}	4.280
	a^{O}_{OClO}	1.8		a^{O}_{OFO}	1.6
h_{ClOO}[a]			h_{FOO}[b]		

[a] $h_{ClOO}=0$.
[b] $h_{FOO}=0$.

for the sake of simplicity. As a consequence, oxygen molecules O_2 cannot be formed as etch products in our MD simulations. However, we believe this does not significantly alter etching characteristics that we are interested in since the attractive interaction between two O atoms is in reality relatively weak compared with other interactions in the Si–O–Cl or Si–O–F systems. A more realistic account for the O–O bond, i.e., more accurate evaluation of v_{OO} and the associated three-body terms, is a subject of future study.

B. Parameter fitting

As we have mentioned earlier, we first make use of previously obtained SW-type potentials for systems that are subsets of general Si–O–F or Si–O–Cl systems. For the convenience of the reader, we have summarized the parameters of the potential functions for Si–F, Si–Cl, and Si–O systems in Appendix A. Interaction with Ar is modeled by the *Moliére* potential, as given in Appendix B. To determine the rest of the parameters, we performed *ab initio* quantum-mechanical calculations based on a density-functional method using "Gaussian."[22] [The employed model chemistry is B3LYP-6-31+G(*d*,*p*).] The obtained potential energy data for various atomic configurations are used to determine the interatomic potential functions. Under the adiabatic assumption for electron dynamics, derivatives of such interatomic potential functions with respect to nucleus positions give interatomic forces.

Based on the potential energy data, we determine the potential-function parameters, using the Levenberg–Marquardt's nonlinear fitting.[23] In this subsection we present how we have determined the fitting parameters for Si–O–Cl systems. A similar fitting method have been used for Si–O–F systems. We take the following three steps: (1) Determination of the O–Cl two-body interaction (i.e., v_{ClO}), (2) determination of the three-body interactions for Cl and O (i.e., h_{ClClO}, h_{ClOCl}, and h_{OClO}), and (3) determination of the Si, O, and Cl three-body interaction (i.e., h_{SiClO}, h_{ClSiO}, and h_{SiOCl}). As mentioned before, h_{SiOO}, h_{ClOO}, and h_{OOO} are assumed to be 0. In what follows, the physical quantities are all nondimensionalized. The employed energy and length units are 50.0 kcal/mol (=2.17 eV) and 2.0951 Å.

1. Two-body potentials

First let us consider the O–Cl two-body potential. As in the case of Si–O systems, the O–Cl binding energy depends on the coordination number (i.e., the number of atoms present in the neighborhood) of the O atom since the valence for covalent binding of oxygen is 2. If there are more than two atoms around an O atom, the bond strengths of the O atom with these surrounding atoms are significantly reduced. To reproduce the valence of oxygen effectively, Watanabe *et al.* employed the bond-softening function $g(i,j)$,[20] which takes values less than unity [and thus reduces the absolute value of potential function $v(i,j)$] if either the ith or jth atom is oxygen and there are more than two atoms in the neighborhood of the oxygen atom.

To give the definition of $g(i,j)$ more precisely, we first define the "coordination number" function $z(i)$ of the ith atom by

$$z(i)=\sum_{l(\neq i)} f_c^{il}(r_{il}), \tag{5}$$

where f_c^{ij} is the cut-off function and the sum is taken over all atoms except for the ith atom. Function f_c^{ij} is defined by

$$f_c^{ij}(r)=\begin{cases} 1 & (r<R_{ij}-D_{ij}), \\ 1-\dfrac{r-R_{ij}+D_{ij}}{2D_{ij}}+\dfrac{\sin\{\pi(r-R_{ij}+D_{ij})/D_{ij}\}}{2\pi} & \\ \qquad (R_{ij}-D_{ij}\leqslant r<R_{ij}+D_{ij}), & \\ 0 & (r\geqslant R_{ij}+D_{ij}). \end{cases} \tag{6}$$

Here R_{ij} and D_{ij} $(R_{ij}\geqslant D_{ij}\geqslant 0)$ are parameters satisfying $R_{ij}=R_{ji}$ and $D_{ij}=D_{ji}$. Clearly the function $z(i)$ represents a "measure" of the number of atoms present in the neighborhood in the ith atom. Indeed if $D_{ij}=0$ and $R_{ij}=R$ (independent of j), then $z(i)$ is equal to the total number of atoms present within the distance R from the ith atom. Parameter R_{ij} essentially represents the scale length of attractive interaction between the ith and jth atoms and D_{ij} is a length parameter introduced to make the function $f_c(z)$ continuously differentiable around $z=R_{ij}$.

In what follows, we consider the effects of valence only for oxygen. In other words, we use $z(i)$ only when the ith atom is oxygen. As mentioned in the preceding subsection, we have assumed for the sake of simplicity that there is no attraction between two O atoms. We now also assume that the presence of oxygen atoms in the neighborhood of an oxygen atom does not reduce the valence of the latter oxy-

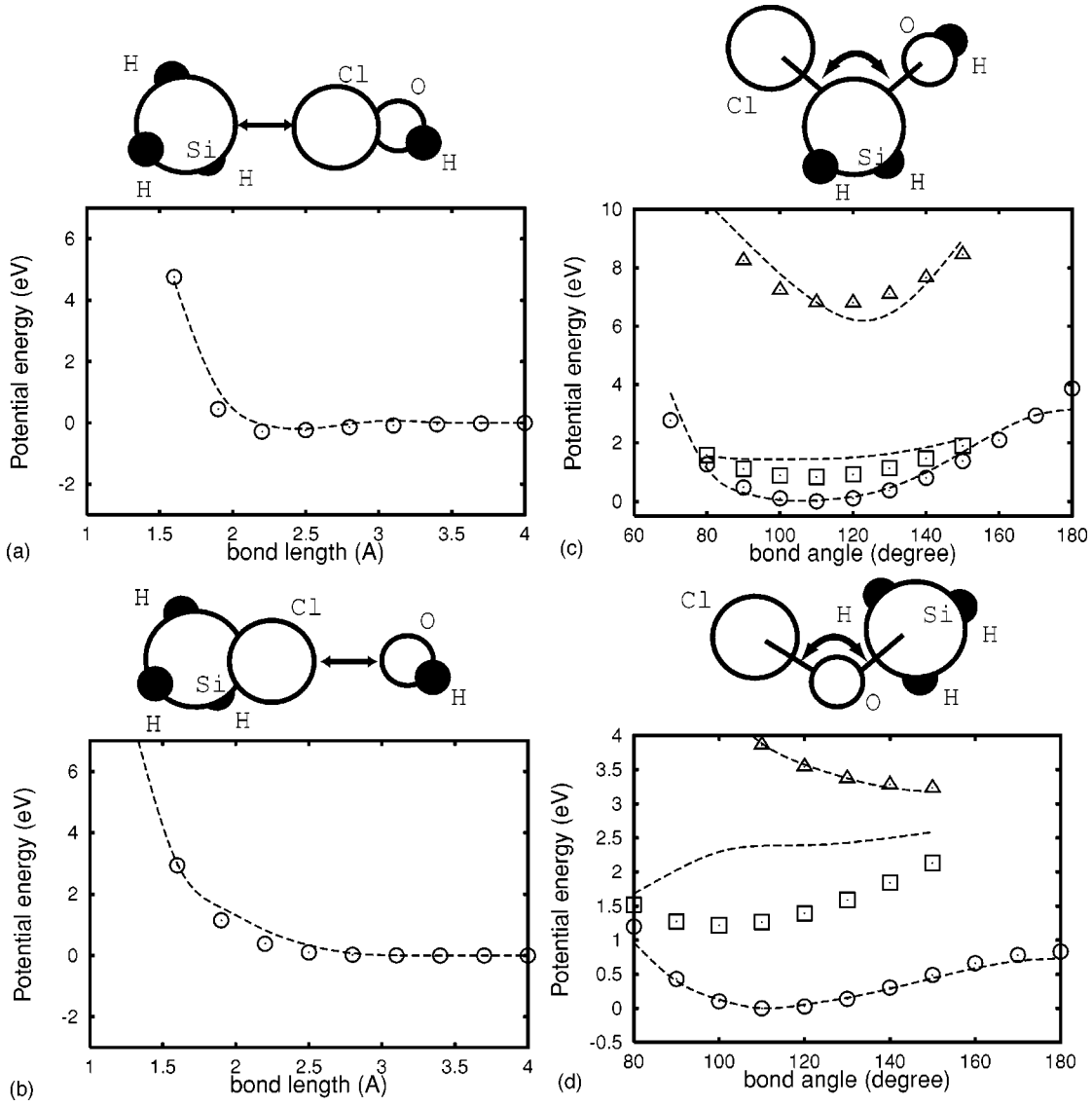

FIG. 3. Potential energy data for Si–O–Cl systems obtained from *ab initio* calculations and our potential functions. The symbols are the same as those used in Fig. 2. In (c) the selected bond lengths are 1.70 Å (△), 2.0658 Å (○), and 2.30 Å (□) for Si–Cl and 1.30 Å (△), 1.659 Å (○), and 1.90 Å (□) for Si–O. In (d) the selected bond lengths are 1.4094 Å (△), 1.7094 Å (○), and 2.0094 Å (□) for O–Si and 1.4266 Å (△), 1.7266 Å (○), and 2.0266 Å (□) for O–Cl.

gen. Therefore, in estimating the coordination number of an oxygen, we count only nonoxygen atoms, which is equivalent to taking the sum for all atoms except for oxygen in Eq. (5) or setting $R_{OO}=D_{OO}=0$ in Eq. (6).

With the coordination numbers thus defined, we use function

$$g(z)=\frac{0.097}{\exp[(1.6-z)/0.3654]+1}\times\exp[0.1344(z-6.4176)^2], \tag{7}$$

to define $g(i,j)$, which is shown in Fig. 1. We set $g(i,j)=g(z(i))$ if the ith atom is oxygen and the jth atom is not oxygen; $g(i,j)=g(z(j))$ if the jth atom is oxygen and the ith atom is not oxygen; $g(i,j)=1$ otherwise (including the case where both the ith and jth atoms are oxygen). This definition satisfies the condition $g(i,j)=g(j,i)$. Note that $g(i,j)$ depends not only on the ith and jth atoms but also all other atoms in the neighborhood. In this sense $v_2(i,j)$ in Eq. (2) is not a true two-body potential but includes effects of multibody interactions.

In order to determine the fitting parameters for v_{OCl}, we calculated the total potential energy for the -O–Cl cluster (i.e., O–Cl cluster with a dangling bond, i.e., the spin multiplicity being $2S+1=2$) by varying the O–Cl bond length, as shown in Fig. 2(a). In this figure, the total potential energy obtained from *ab initio* calculations is indicated by empty circles. We adjusted the value of A_{OCl} to better represent the known experimental value of binding energy 2.09 eV for the O–Cl bond of OCl_2 molecule (which is slightly different from the O–Cl binding energy of -O–Cl cluster). The determined parameters for O–Cl are summarized in Table I. The obtained pair function $v_{ClO}(r)$ with the coordination number $z_O=2$ are given as dashed curves in Fig. 2(a).

TABLE II. Parameters of the three-body interatomic potential functions for Si–O–Cl and Si–O–F systems.

Si–O–Cl			Si–O–F		
h_{SiClO}	λ_{SiClO}	214	h_{SiFO}	λ_{SiFO}	1070
[Eq. (3)]	γ^{Si}_{SiClO}	1.12	[Eq. (3)]	γ^{Si}_{SiFO}	0.908
	γ^{O}_{SiClO}	3.24		γ^{O}_{SiFO}	4.45
	a^{Si}_{SiClO}	1.8		a^{Si}_{SiFO}	1.6
	a^{O}_{SiClO}	1.8		a^{O}_{SiFO}	1.6
h_{ClSiO}	λ_{ClSiO}	33.5	h_{FSiO}	λ_{FSiO}	3.13
[Eq. (4)]	γ^{Cl}_{ClSiO}	0.295	[(Eq. 4)]	γ^{F}_{FSiO}	0.424
	γ^{O}_{ClSiO}	1.63		γ^{O}_{FSiO}	1.22
	a^{Cl}_{ClSiO}	1.4		a^{F}_{FSiO}	1.4
	a^{O}_{ClSiO}	1.4		a^{O}_{FSiO}	1.4
	$\cos\theta^{0}_{ClSiO}$	0.0575		$\cos\theta^{0}_{FSiO}$	0.396
	α_{ClSiO}	2.31		α_{FSiO}	3.15
h_{SiOCl}	λ_{SiOCl}	10.3	h_{SiOF}	λ_{SiOF}	47.8
[Eq. (4)]	γ^{Si}_{SiOCl}	0.723	[Eq. (4)]	γ^{Si}_{SiOF}	0.653
	γ^{Cl}_{SiOCl}	0.564		γ^{F}_{SiOF}	1.56
	a^{Si}_{SiOCl}	1.4		a^{Si}_{SiOF}	1.4
	a^{Cl}_{SiOCl}	1.4		a^{F}_{SiOF}	1.4
	$\cos\theta^{0}_{SiOCl}$	−0.438		$\cos\theta^{0}_{SiOF}$	−0.263
	α_{SiOCl}	1.05		α_{SiOF}	1.18

2. Three-body potentials for two different species

Second we determine the three-body interactions for clusters among Cl and O atoms, i.e., the parameters for h_{ClClO}, h_{ClOCl}, and h_{OClO}. The total potential energy data were obtained for clusters Cl_2OH and Cl_2O from *ab initio* calculations as functions of some bond lengths and bond angles, as plotted in Fig. 2. (Hydrogen atoms are used to terminate extra bonds.) In Fig. 2(b), the total potential energy is plotted by empty circles as a function of the distance between a single Cl atom and the Cl atom of ClOH with the bond angle $\theta_{ClClO}=180°$. The ClOH cluster configuration is fixed when the Cl–Cl bond length is varied, i.e., the bond lengths for Cl–O and O–H are $r_{ClO}=1.7269$ Å and $r_{OH}=0.9723$ Å, and the bond angle around O is $\theta_{ClOH}=103.3488°$.

Similarly, in Fig. 2(c), the total energy is plotted by empty circles as a function of the distance between a Cl atom of Cl_2 molecule and the oxygen of an OH cluster with $\theta_{ClClO}=180°$, $\theta_{ClOH}=103.3488°$, $r_{ClCl}=2.045$ Å (which is close to the bond length of most stable Cl_2), and $r_{OH}=0.9723$ Å. In Fig. 2(d) the distance between two Cl atoms and that between Cl–O are taken to be the same and varied simultaneously. The fixed parameters are $\theta_{ClClO}=180°$, $\theta_{ClOH}=103.3488°$, and $r_{OH}=0.9723$ Å as in Fig. 2(b). The bond angle at O for OCl_2 are varied in Fig. 2(e) with both Cl–O bond lengths being 1.40 Å (empty triangles), 1.7343 Å (empty circles), and 2.00 Å (empty squares). The parameters for h_{ClClO} [given by Eq. (3)] and h_{ClOCl} [given by Eq. (4)] are determined simultaneously by fitting the potential functions to the data given in Figs. 2(b)–2(e).

Similarly the parameters for h_{OClO} are obtained from *ab initio* data for $Cl(OH)_2$ as shown in Fig. 2(f), where the distance between O of an OH cluster and Cl was varied. Here the fixed parameters of the "separated" OH cluster are $\theta_{HOCl}=103.3488°$ and $r_{OH}=0.9723$ Å. The other fixed parameters are $\theta_{OClO}=180°$, $\theta_{ClOH}=103.3488°$, $r_{OCl}=1.7269$ Å, and $r_{OH}=0.9723$ Å for the ClOH cluster. All the atoms in H–O–Cl–O–H are on a single plane and both hydrogen atoms are on the same side against the straight O–Cl–O axis, as shown in Fig. 2(f). The obtained parameters are given in Table I. The total potential energy calculated from the obtained potential functions $v_2(i,j)$ and $v_3(i,j,k)$ are shown by dashed curves in Fig. 2.

In Fig. 2(a)–2(d) and 2(f), we take zero energy to be the system energy when the bond length in question is infinity. In a figure where the total potential energy is plotted against a bond angle [such as Fig. 2(e)], the zero energy is taken to be the minimum of the plotted energy. In all energy figures presented in this paper, we follow this convention regarding the zero energy level.

3. Three-body potentials for three different species

Finally the three-body potentials for Si, O, and Cl atoms, i.e., the parameters in h_{SiClO}, h_{ClSiO}, and h_{SiOCl}, are determined. Potential energy data obtained from *ab initio* calculations for SiH_3–Cl–OH, Cl–SiH_2–OH, and Cl–O–SiH_3 clusters are plotted in Fig. 3. In Fig. 3(a), the total potential energy is plotted by empty circles as a function of the Si–Cl bond length for SiH_3–Cl–OH. Here one of the H atoms of SiH_4 with $r_{SiH}=1.4798$ Å is replaced by ClOH [whose atomic configuration is the same as that in Fig. 2 (f)], where $\theta_{HSiH}=\theta_{HSiCl}=109.471\,22°[=\cos^{-1}(-1/3)]$, and $\theta_{SiClO}=180°$. One of the H atoms of SiH_3, Si, and Cl–O–H span a single plane and these two H atoms are on the same side against the straight Si–Cl–O axis.

In Fig. 3(b) the total energy is plotted as a function of the Cl–O bond length for a cluster similar to that in Fig. 3(a). Here the Si–Cl bond length is taken to be 2.0829 Å. The other parameters in Fig. 3(b) is the same as those in Fig. 3(a). The configuration of $SiClH_3$ used here is close to its most stable configuration.

In Fig. 3(c), the Si–H and O–H bond lengths are taken to be $r_{SiH}=1.48$ Å and $r_{OH}=0.9636$ Å with bond angles $[\theta_{HSiH}=\theta_{HSiO}=\theta_{HSiCl}=109.471\,22°(=\cos^{-1}(-1/3))]$ and $\theta_{SiOH}=103.3488°$. The total energy is plotted as a function of bond angle θ_{ClSiO} for the following three cases: $r_{SiCl}=1.70$ Å and $r_{SiO}=1.30$ Å (empty triangles), $r_{SiCl}=2.0658$ Å and $r_{SiO}=1.659$ Å (empty circles), and $r_{SiCl}=2.30$ Å and $r_{SiO}=1.90$ Å (empty squares). As shown in the figure, H(left-bottom)–Si–O–H(top) atoms span a single plane, which is perpendicular to the plane formed by Cl–Si–H(right bottom) atoms.

In Fig. 3(d) one of the H atoms of SiH_4 is replaced by the O atom of an OCl cluster [$r_{SiH}=1.48$ Å and $\theta_{HSiH}=\theta_{HSiO}=109.471\,22°(=\cos^{-1}(-1/3))$] and the total energy is plotted as a function of bond angle θ_{ClOSi} for three cases: $r_{ClO}=1.4266$ Å and $r_{SiO}=1.4094$ Å (empty triangles), $r_{ClO}=1.7266$ Å and $r_{SiO}=1.7094$ Å (empty circles), and $r_{ClO}=2.0266$ Å and $r_{SiO}=2.0094$ Å (empty squares). The atomic configuration used for the energy calculation is such that Cl–O–Si and one of the H atoms form a single plane.

The obtained fitting parameters are summarized in Table II. The potential energy calculated from the obtained poten-

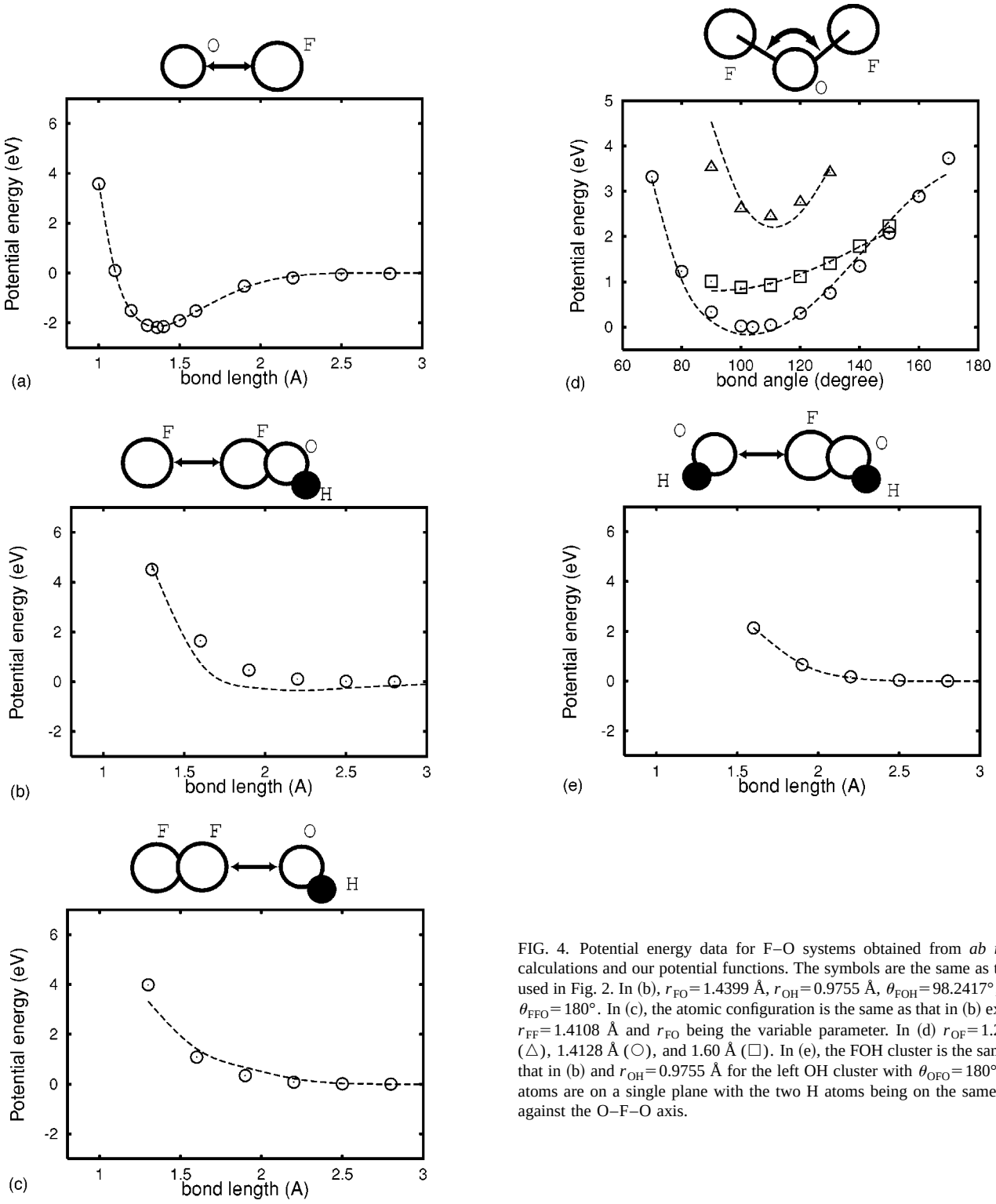

FIG. 4. Potential energy data for F–O systems obtained from *ab initio* calculations and our potential functions. The symbols are the same as those used in Fig. 2. In (b), $r_{FO}=1.4399$ Å, $r_{OH}=0.9755$ Å, $\theta_{FOH}=98.2417°$, and $\theta_{FFO}=180°$. In (c), the atomic configuration is the same as that in (b) except $r_{FF}=1.4108$ Å and r_{FO} being the variable parameter. In (d) $r_{OF}=1.20$ Å (△), 1.4128 Å (○), and 1.60 Å (□). In (e), the FOH cluster is the same as that in (b) and $r_{OH}=0.9755$ Å for the left OH cluster with $\theta_{OFO}=180°$. All atoms are on a single plane with the two H atoms being on the same side against the O–F–O axis.

tial functions are plotted as dashed curves in Fig. 3. While the agreement between the *ab initio* data and fitting curves are good for most cases, we see some discrepancies in Fig. 3(c) and 3(d), especially when the bond length is larger than the most stable length. The nonlinear fitting we had employed was biased toward more stable states, so that the fitting parameters were selected to obtain the best fit near the energy minimum. Since the discrepancy appears only when the bond lengths are much larger than the optimal lengths (and therefore, the system is less stable), we expect that the discrepancy does not significantly alter the dynamics of molecules under our simulation conditions (i.e., etching by relatively high–energy beams). To some extent such discrepancy is unavoidable as we assume some particular functional forms such as those given by Eqs. (2)–(4) to reduce the number of free parameters to a manageable level.

A similar fitting method was used to determine the interatomic potential parameters for Si–O–F systems, as shown

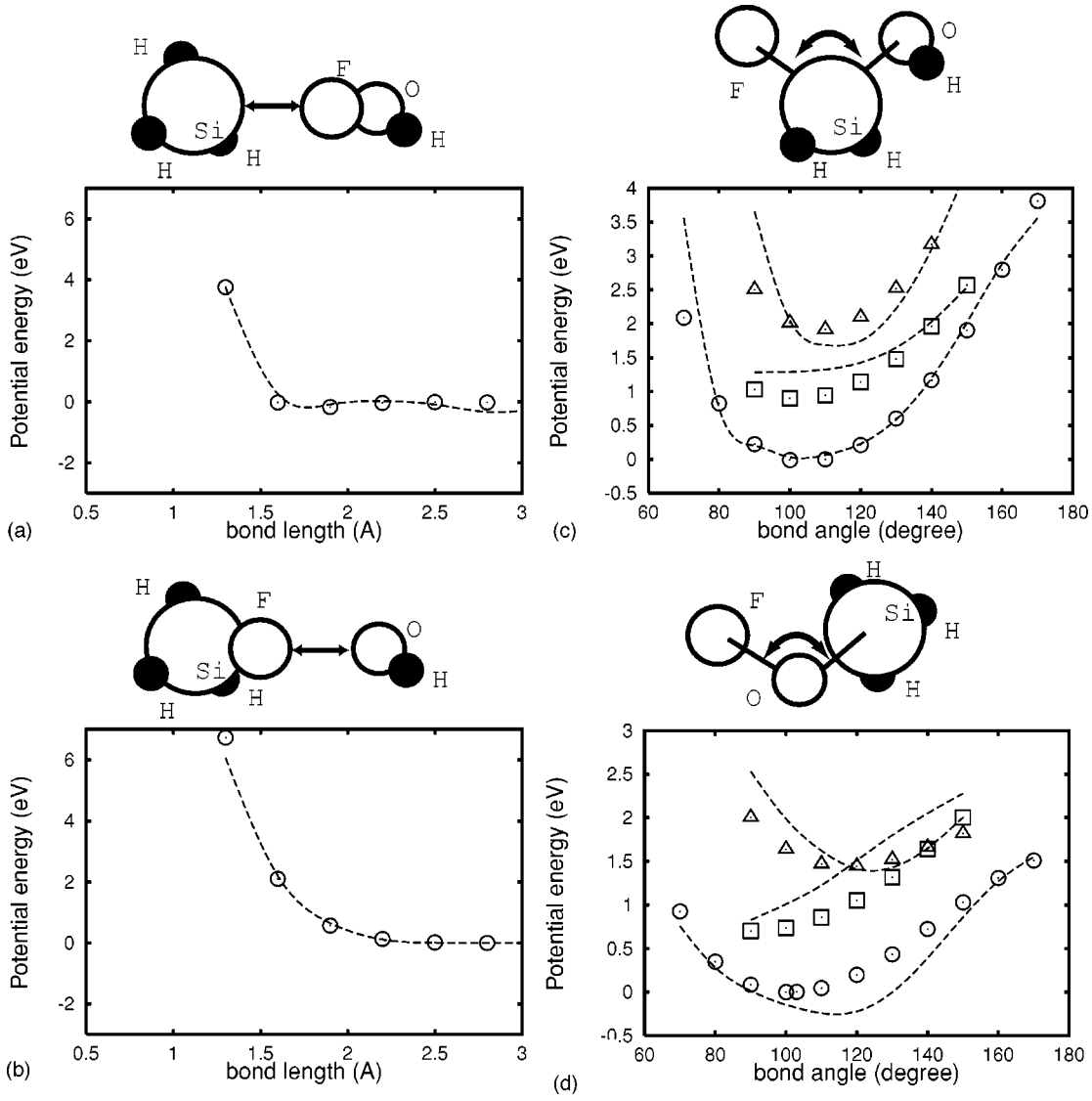

FIG. 5. Potential energy data for Si–O–F systems obtained from *ab initio* calculations and our potential functions. The symbols are the same as those used in Fig. 2 and the atomic configurations are similar to those in the corresponding figures in Fig. 3. In (a) and (b), $r_{SiH}=1.48$ Å, $r_{OH}=0.9755$ Å, $r_{OF}=1.4399$ Å, $r_{SiF}=1.6318$ Å, $\theta_{SiFO}=180°$, and $\theta_{FOH}=98.2417°$. In (c), $r_{SiH}=1.48$ Å, $r_{OH}=0.9636$ Å, and $\theta_{SiOH}=119.9428$. The selected bond lengths are $r_{SiF}=1.42$ Å (△), 1.6277 Å (○), 1.82 Å (□), and $r_{SiO}=1.45$ Å (△), 1.6527 Å (○), 1.85 Å (□). In (d), $r_{SiH}=1.48$ Å, and the selected bond lengths are $r_{OSi}=1.52$ Å (△), 1.7232 Å (○), 1.92 Å (□), and $r_{OF}=1.26$ Å (△), 1.4608 Å (○), 1.66 Å (□).

in Figs. 4 and 5. The obtained parameters are also summarized in Tables I and II. The total potential energy calculated from the obtained potential functions $v_2(i,j)$ and $v_3(i,j,k)$ are given by dashed curves in Figs. 4 and 5. The binding energies and bond lengths are also calculated from the obtained potential sets, which are given in the Table III. Here the binding energy and bond length are defined as the energy and position of the energy minimum of the corresponding two–body potential.

TABLE III. Binding energies and bond lengths.

	Binding energy		
	(eV)	(kcal/mol)	Bond length (Å)
Si–Si	2.17	50.0	2.35
Si–O	4.14	95.4	1.61
Si–Cl	3.96	91.2	2.06
Cl–Cl	2.47	56.9	1.96
Cl–O	2.09	48.2	1.62
Si–F	5.72	132	1.60
F–F	1.66	38.3	1.43
F–O	2.18	50.2	1.36

III. SAMPLE SIMULATIONS

Some MD simulations based on the new potential sets are presented in this section. In the simulations, target atoms are placed in a simulation cell with periodic boundary conditions in the horizontal directions. The target surface is a square of side length 21.7 Å (the area is 472 Å^2) with a monolayer initially including 32 Si atoms for the silicon target and 32 Si and 64 O atoms for the oxide target. Initially the target materials contain 16 monolayers (i.e., 512 Si atoms) for the Si target and 12 monolayers (i.e., 384 Si atoms and 768 O atoms, totaling 1152 atoms) for the oxide target,

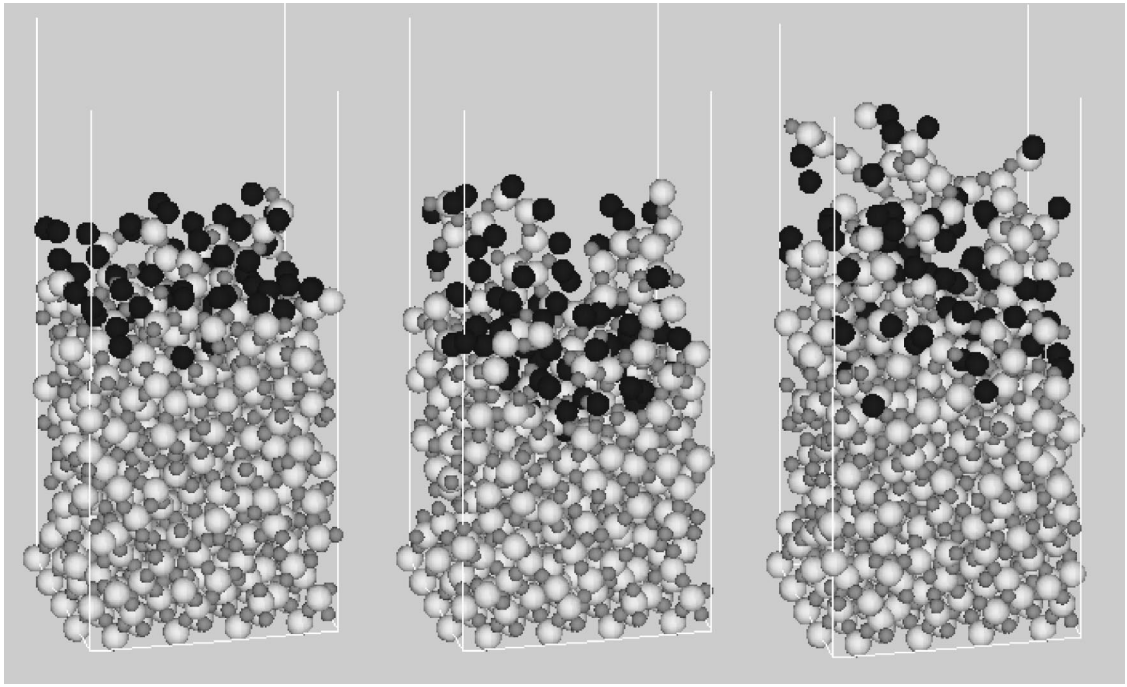

FIG. 6. Typical surface structures during Cl beam etching. Large white spheres are Si atoms, small gray spheres are O atoms, and big black spheres are Cl atoms. The beam is normal to the target surface and the impact energy is 50, 100, and 150 eV from left to right. The simulation surface size is 21.7 Å×21.7 Å.

the depths of which are 21 Å for Si and 32 Å for SiO_2. The initial target temperature is 300 °K and the atoms in the bottom layer are rigidly fixed to prevent the drift of the entire simulation cell.

Energetic atoms are injected from randomly selected horizontal locations just above the target in the direction normal to the surface. It is sometimes more convenient to measure the dose of impinging particles in units of monolayer (ML), with 1 ML corresponding to 32 impinging particles in both Si and oxide cases in our simulation. Since energetic ions impinging on the surface are expected to be neutralized near the target surface due to an Auger emission process, we

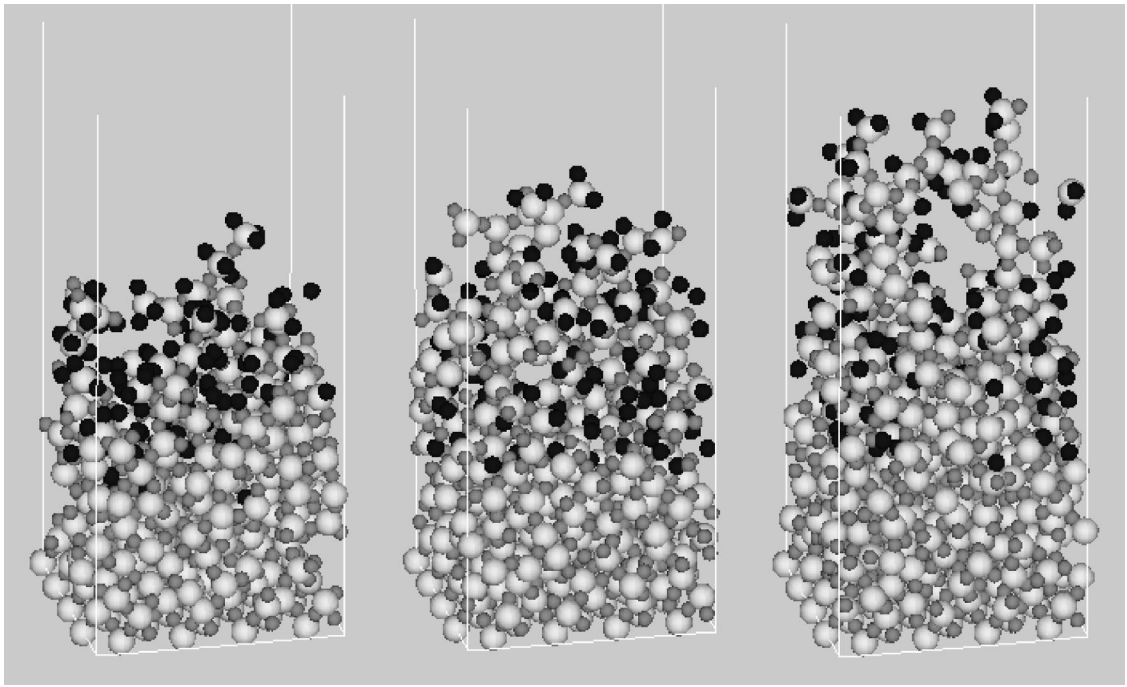

FIG. 7. Typical surface structures during F beam etching. Large white spheres are Si atoms, small gray spheres are O atoms, and small black spheres are F atoms. The beam is normal to the target surface and the impact energy is 50, 100, and 150 eV from left to right. The simulation surface size is 21.7 Å×21.7 Å.

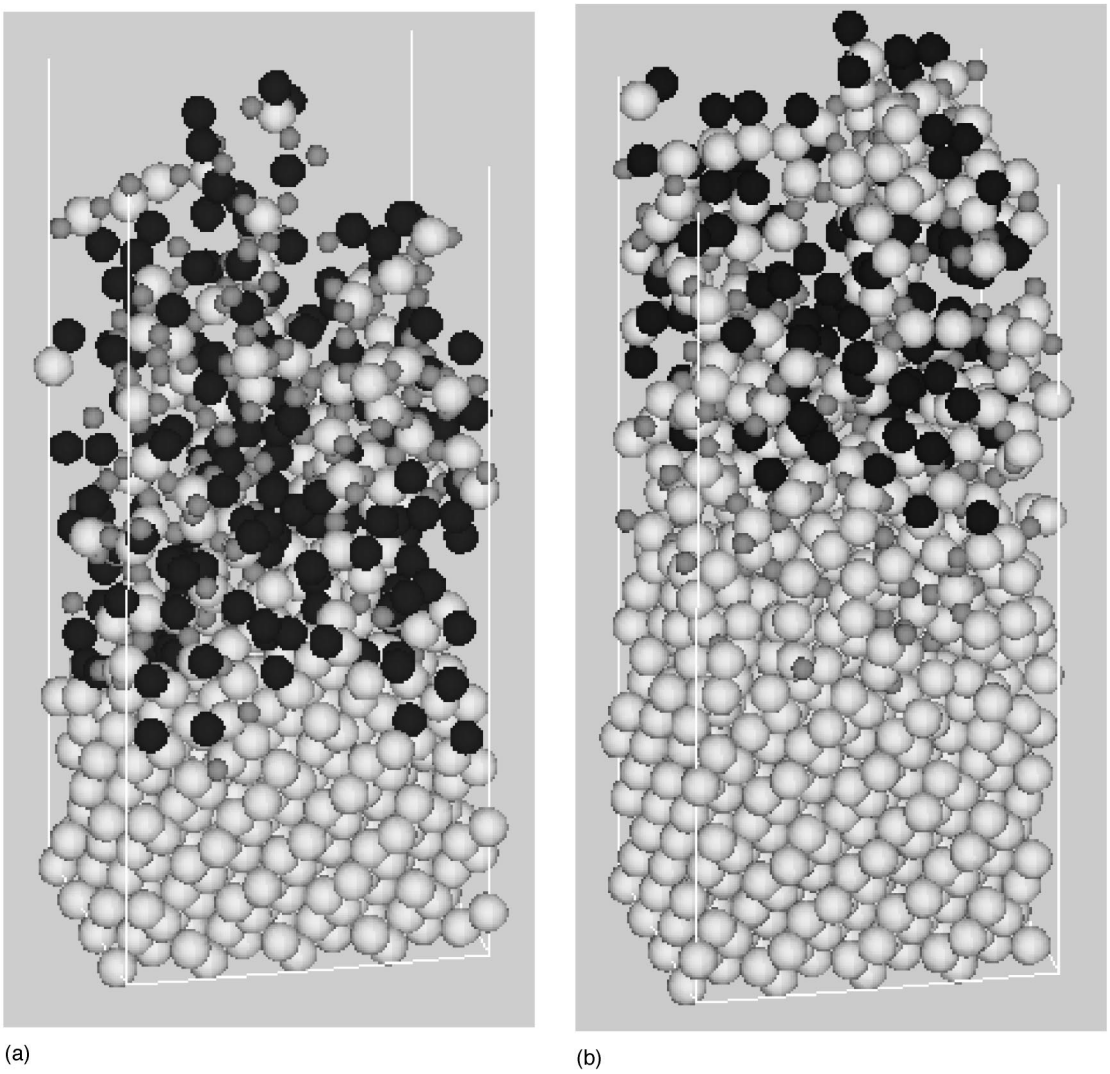

FIG. 8. Typical surface structures of silicon target during 100 eV Cl beam etching in an oxygen atmosphere after about 10 ML Cl injections. Large white spheres are Si atoms, small gray spheres are O atoms, and big black spheres are Cl atoms. The simulation surface size is 21.7 Å×21.7 Å. (a) 20 oxygen atoms with low energy (1 eV) are supplied to the surface vertically before each Cl impact. (b) 100 eV O and Cl atoms vertically impinge upon the surface in an alternating manner.

only consider charge-neutral atoms as injected species. It is also assumed that the target surface is kept charge-neutral during the process.

After injection of each atom, we let the system evolve for 0.7 ps under the constant total-energy conditions. Most transient processes such as rapid release of the kinetic energy of injected atom to the target occur during this period. We then artificially cool the entire system (by decreasing the velocities of all atoms) for 0.3 ps to reduce the target temperature to the initial temperature (i.e., 300 °K) in order to prevent the system from being unrealistically heated up. The bombardment process by a single energetic particle is repeated about 1000 times (i.e., about 31 ML) to increase statistics for the measurement of macroscopic parameters such as sputtering yields.

First we discuss simulation results of $Si–SiO_2$ selective etching by halogens beams.[11] Figures 6 and 7 show typical surface morphologies of an SiO_2 target during Cl and F mono-energetic beam etching. These figures are obtained after 10 ML atomic bombardment of the clean targets in simulations. The impact energy is 50, 100, and 150 eV from left to right. As shown in these figures, the halogenated layer becomes thicker as the impact energy increases. Also the halogenated layer is thicker for F injection than for Cl injection with the same impact energy. For example, in the case of the 50 eV Cl beam, most Cl atoms are adsorbed only on the top surface of the oxide target, as shown in Fig. 6, whereas F atoms penetrate deeper into the oxide target with the same impact energy, as shown in Fig. 7. This is because the Si–F bond is stronger than the Si–Cl bond and the atomic size of F is smaller than that of Cl. For more details, the reader is referred to Ref. 11.

Second, let us consider Si etching in an oxygen atmosphere. In some $Si–SiO_2$ selective etching by Cl, oxygen is added to chlorine plasmas to removes hydrocarbon fragments sputtered from the photoresist.[24] (Such hydrocarbon fragments increase the SiO_2 etch rate and thus reduce $Si–SiO_2$ etch selectivity.) However, added O atoms can also

TABLE IV. Parameters of the two-body potentials for Si–O systems obtained by Stillinger and Weber (for the Si–Si pair) (Ref. 1) and by Watanabe *et al.* (for Si–O and O–O pairs) (Ref. 20).

Si–O–Cl and Si–O–F		
v_{SiSi} [Eq. (2)]	A_{SiSi}	7.049 556 277
	B_{SiSi}	0.602 224 558 4
	C_{SiSi}	1.0
	p_{SiSi}	4
	q_{SiSi}	0
	a_{SiSi}	1.8
v_{SiO} [Eq. (2)]	A_{SiO}	115.364 065 913
	B_{SiO}	0.909 444 279 3
	C_{SiO}	1.0
	p_{SiO}	2.587 59
	q_{SiO}	2.393 70
	a_{SiO}	1.4
	R_{SiO}	1.3
	D_{SiO}	0.1
v_{OO} [Eq. (2)]	A_{OO}	−12.292 427 744
	B_{OO}	0
	C_{OO}	1.0
	p_{OO}	0
	q_{OO}	2.244 32
	a_{OO}	1.25

TABLE V. Parameters of the three-body potentials for Si–O systems obtained by Watanabe *et al.* (Ref. 20). Note that the parameters for the Si–Si–Si triplet are different from those originally given by Stillinger and Weber (Ref. 1).

Si–O–Cl and Si–O–F		
h_{SiSiSi} [Eq. (4)]	λ_{SiSiSi}	16.404
	γ^{Si}_{SiSiSi}	1.0473
	a^{Si}_{SiSiSi}	1.8
	$\cos\theta^0_{SiSiSi}$	−1/3
	α_{SiSiSi}	1.0
h_{SiSiO} [Eq. (4)]	λ_{SiSiO}	10.667
	γ^{Si}_{SiSiO}	1.939 73
	γ^{O}_{SiSiO}	0.25
	a^{Si}_{SiSiO}	1.9
	a^{O}_{SiSiO}	1.4
	$\cos\theta^0_{SiSiO}$	−1/3
	α_{SiSiO}	1.0
h_{SiOSi} [Eq. (4)]	λ_{SiOSi}	2.9572
	γ^{Si}_{SiOSi}	0.717 73
	a^{Si}_{SiOSi}	1.4
	$\cos\theta^0_{SiOSi}$	−0.615 523 8
	α_{SiOSi}	1.0
h_{OSiO} [Eq. (4)]	λ_{OSiO}	3.1892
	γ^{O}_{OSiO}	0.3220
	a^{O}_{OSiO}	1.65
	$\cos\theta^0_{OSiO}$	−1/3
	α_{OSiO}	1.0
h_{SiOO}[a]		
h_{OOO}[b]		

[a] $h_{SiOO}=0$.
[b] $h_{OOO}=0$.

TABLE VI. Parameters of the two-body potentials for Si–Cl (Refs. 1 and 2) and Si–F (Ref. 3) systems.

Si–O–Cl			Si–O–F		
v_{SiCl} [Eq. (2)]	A_{SiCl}	28.0	v_{SiF} [Eq. (2)]	A_{SiF}	21.234 141 38
	B_{SiCl}	0.67		B_{SiF}	0.569 547 643 3
	C_{SiCl}	1.3		C_{SiF}	1.3
	p_{SiCl}	2.2		p_{SiF}	3
	q_{SiCl}	0.9		q_{SiF}	2
	a_{SiCl}	1.8		a_{SiF}	1.8
v_{ClCl} [Eq. (2)]	A_{ClCl}	8.611	v_{FF} [Eq. (2)]	A_{FF}	0.522 76
	B_{ClCl}	0.789		B_{FF}	0.112 771
	C_{ClCl}	0.5795		C_{FF}	0.579 495
	p_{ClCl}	6		p_{FF}	8
	q_{ClCl}	5		q_{FF}	4
	a_{ClCl}	2.0862		a_{FF}	2.086 182

significantly reduce the Si etch rate if surface oxidation becomes too high. Typical Si surfaces obtained from MD simulations under such conditions are shown in Fig. 8. In the simulations, 20 oxygen atoms are injected to the Si surface at random positions in the normal direction with sufficiently low energy (1 eV) before each 100 eV Cl injection. We observe in Fig. 8(a) that low–energy oxygen atoms, which would be adsorbed just on the Si surface without the Cl beam injection, formed a relatively deep chlorinated layer due to

TABLE VII. Parameters of the three-body potentials obtained by Stillinger and Weber for Si–Cl systems (Refs. 1 and 2) and by Feil *et al.* for Si–F systems (Ref. 3).

Si–O–Cl			Si–O–F		
h_{SiClCl} [Eq. (3)]	λ_{SiClCl}	15	h_{SiFF} [Eq. (3)]	λ_{SiFF}	3.5
	γ^{Si}_{SiClCl}	1.0		γ^{Si}_{SiFF}	1.0
	γ^{Cl}_{SiClCl}	1.0		γ^{F}_{SiFF}	1.0
	a^{Si}_{SiClCl}	1.8		a^{Si}_{SiFF}	1.8
	a^{Cl}_{SiClCl}	1.8		a^{F}_{SiFF}	1.8
h_{SiClSi} [Eq. (3)]	λ_{SiClSi}	50	h_{SiFSi} [Eq. (3)]	λ_{SiFSi}	50
	γ^{Si}_{SiClSi}	1.0		γ^{Si}_{SiFSi}	1.3
	a^{Si}_{SiClSi}	1.8		a^{Si}_{SiFSi}	1.8
h_{SiSiCl} [Eq. (4)]	λ_{SiSiCl}	15	h_{SiSiF} [Eq. (4)]	λ_{SiSiF}	15
	γ^{Si}_{SiSiCl}	1.0		γ^{Si}_{SiSiF}	1.0
	γ^{Cl}_{SiSiCl}	1.0		γ^{F}_{SiSiF}	1.0
	a^{Si}_{SiSiCl}	1.8		a^{Si}_{SiSiF}	1.8
	a^{Cl}_{SiSiCl}	1.8		a^{F}_{SiSiF}	1.8
	$\cos\theta^0_{SiSiCl}$	−1/3		$\cos\theta^0_{SiSiF}$	−1/3
	α_{SiSiCl}	1.0		α_{SiSiF}	1.0
h_{ClSiCl}[a]			h_{FSiF}[b]		
h_{ClClCl}[c]			h_{FFF}[d]		

[a] $h_{ClSiCl}(r,s,\theta)=[30(\cos\theta-\cos 103°)^2-0.5]\exp[1/(r-1.8)+1/(s-1.8)]$
[b] $h_{FSiF}(r,s,\theta)=[24(\cos\theta-\cos 103°)^2-3.2]\exp[1(r-1.8)+1/(s-1.8)]$
[c] $h_{ClClCl}(r,s,\theta)=3(rs)^{-2.056}\exp[0.5795/(r-2.0862)+0.5795/(s-2.0862)]+23.778(2.0-\cos^2\theta)\exp[1.7386/(r-1.6226)+1.7386/(s-1.6226)]$
[d] $h_{FFF}(r,s,\theta)=0.0818182(rs)^{-4}\exp[0.579\,495/(r-2.086\,182)+0.579\,495/(s-2.086\,182)]+19.1475(2.0-\cos^2\theta)\exp[1.738\,485/(r-1.622\,586)+1.738\,485/(s-1.622\,586)]$.

TABLE VIII. Parameters of the pseudo-Moliére potentials.

i-j	A_{ij}	B_{ij}	C_{ij}	p_{ij}	q_{ij}	a_{ij}
Ar–Ar	−5.64	0	0.835	0	4.27	1.6
Ar–Cl	−5.47	0	0.818	0	4.25	1.6
Ar–Si	−4.90	0	0.766	0	4.18	1.6
Ar–F	−3.73	0	0.665	0	4.05	1.6
Ar–O	−3.46	0	0.641	0	4.02	1.6
Ar–C	−2.84	0	0.589	0	3.95	1.6

mixing caused by energetic Cl impacts. The Si sputtering yield (i.e., the number of Si atoms removed from the target per Cl impact) estimated by the simulations (averaged over 10–15 ML Cl impacts) is 0.10 per Cl impact. This is close to the Si sputtering yield of a SiO_2 surface by 100 eV pure Cl injection ($\simeq$0.11, as given in Ref. 11), rather than that of the same silicon surface by 100 eV pure Cl injection ($\simeq$0.46[11]).

Shown in Fig. 8(b) is a typical Si surface upon which 100 eV O and Cl atoms impinge alternately. Despite the high oxygen impinging energy, the resulting surface structure is similar to that shown in Fig. 8(a) after sufficient Cl and O fluence. The obtained Si sputtering yield (per Cl impact) is 0.16, which is again close to the Si sputtering yield of SiO_2 surface by 100 eV pure Cl injection. We have also performed MD simulations of SiO_2 etching by 100 eV Cl injection in an oxygen atmosphere, similar to those given in Fig. 8. It is found that oxide etch rates are not much influenced by the presence of extra oxygen.

IV. SUMMARY

We have derived classical interatomic potential sets for Si–O–Cl and Si–O–F systems that are suitable for MD simulation study for plasma–surface interactions during Si and SiO_2 plasma or beam etching processes by halogens (Cl or F). The new results are summarized in Tables I and II. We have also presented some MD simulation results for Si–SiO_2 selective beam etching and Si etching by a Cl beam in an oxygen atmosphere. Details of MD simulations for the former have been given in Ref. 11. As demonstrated in our simulations as well as earlier simulation results by various authors, atomic–scale MD simulation is a useful technique that helps us understand surface reaction dynamics during plasma processing.

ACKNOWLEDGMENT

This work was supported in part by Semiconductor Leading Edge Technologies, Inc. (SELETE).

APPENDIX A

In Tables IV–VII , parameters of the previously obtained potential functions for Si–F, Si–Cl, and Si–O systems are summarized for the convenience of the reader.

APPENDIX B

The Moliére repulsive pair potential[21] is given by

$$V(r)=\frac{Z_1Z_2e^2}{4\pi\varepsilon_0 r}\{0.35\exp(-0.3r/a)+0.55\exp(-1.2r/a)+0.10\exp(-6.0r/a)\},$$

with

$$a=0.885a_0(Z_1^{1/2}+Z_2^{1/2})^{-2/3},$$

and $a_0(=5.291\,772\,49\times10^{-11})$ being Forsov screening length and Bohr radius. Here Z_1 and Z_2 are the atomic numbers. To simplify the coding, we fit Eq. (2) to the Moliére potential and used the obtained ''pseudo''-Moliére to describe interaction between Ar and other atoms. The fitting parameters are shown in Table VIII.

[1] F. H. Stillinger and T. A. Weber, Phys. Rev. B **31**, 5262 (1985); J. Chem. Phys. **88**, 5123 (1988); Phys. Rev. Lett. **62**, 2144 (1989).
[2] T. A. Weber and F. H. Stillinger, J. Chem. Phys. **92**, 6239 (1990).
[3] H. Feil, J. Dieleman, and B. J. Garrison, J. Appl. Phys. **74**, 1303 (1993).
[4] R. A. Stansfield, K. Broomfield, and D. C. Clary, Phys. Rev. B **39**, 7680 (1989).
[5] R. Smith, D. E. Harrison, Jr., and B. J. Garrison, Phys. Rev. B **40**, 93 (1989).
[6] T. A. Schoolcraft and B. J. Garrison, J. Vac. Sci. Technol. A **8**, 3496 (1990); J. Am. Chem. Soc. **113**, 8221 (1991).
[7] M. E. Barone and D. B. Graves, J. Appl. Phys. **77**, 1263 (1995); **78**, 6604 (1995).
[8] B. A. Helmer and D. B. Graves, J. Vac. Sci. Technol. A **15**, 2252 (1997); **17**, 2759 (1999).
[9] D. E. Hanson, A. F. Voter, and J. D. Kress, J. Appl. Phys. **82**, 3552 (1997).
[10] N. A. Kubota, D. J. Economou, and S. J. Plimpton, J. Appl. Phys. **83**, 4055 (1998).
[11] H. Ohta and S. Hamaguchi, J. Vac. Sci. Technol. A (unpublished).
[12] P. C. Weakliem, C. J. Wu, and E. A. Carter, Phys. Rev. Lett. **69**, 200 (1992).
[13] P. C. Weakliem and E. A. Carter, J. Chem. Phys. **98**, 737 (1993).
[14] L. E. Carter, S. Khodabandeh, P. C. Weakliem, and E. A. Carter, J. Chem. Phys. **100**, 2277 (1994).
[15] D. E. Hanson, A. F. Voter, and J. D. Kress, J. Chem. Phys. **110**, 5983 (1999); J. Vac. Sci. Technol. A **17**, 1510 (1999).
[16] C. F. Abrams and D. B. Graves, J. Vac. Sci. Technol. A **16**, 3006 (1998).
[17] A. Kubota and D. J. Economou, IEEE Trans. Plasma Sci. **27**, 1416 (1999).
[18] G. J. Kramer, N. P. Farragher, B. W. H. van Beest, and R. A. van Santen, Phys. Rev. B **43**, 5068 (1991).
[19] Z. Jiang and R. A. Brown, Phys. Rev. Lett. **74**, 2046 (1995).
[20] T. Watanabe, H. Fujiwara, H. Noguchi, T. Hosino, and I. Ohdomari, Jpn. J. Appl. Phys. Lett. **38**, 366 (1999).
[21] I. Torrens, *Interatomic potentials* (Academic, New York, 1972).
[22] J. B. Foresman and A. Frisch, *Exploring Chemistry with Electronic Structure Methods* (Gaussian, Inc., Pittsburgh, 1996).
[23] W. H. Press, S. A. Teukolsky, W. T. Vetterling, and B. P. Flannery, *Numerical Recipes in C* (Cambridge University Press, 1988).
[24] S. C. McNevin, J. Vac. Sci. Technol. B **8**, 1185 (1990).